

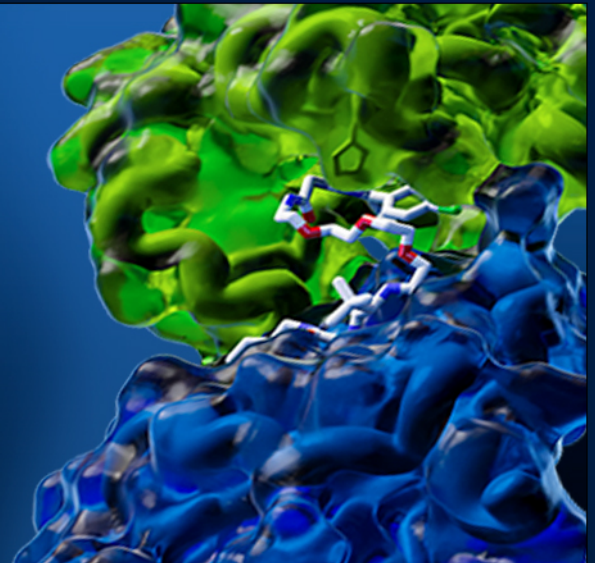
Analytical Exchange Webinar

## Accelerating Protein Analysis Throughput at Boehringer Ingelheim

October 3, 2023

3pm BST | 4pm CEST | 10am EDT | 7am PDT

[Register](#)



### Advancing Drug Discovery with Targeted Protein Degradation

Unlike traditional drug discovery, which focuses on inhibiting or activating proteins, targeted protein degradation (TPD) offers a more precise and efficient way to alter cellular pathways. However, TPD faces several challenges that need to be overcome to reach its full potential, including reducing the bottleneck of quantitative protein analysis.

In this upcoming webinar, the team at Boehringer Ingelheim present their recent real-world TPD project examples and in-depth analysis, covering insights on device and consumable management and optimized assay setups to increase protein analysis throughput.

#### Speakers



**Andrea Stingu**  
Lab Scientist  
Boehringer Ingelheim

**Johannes Wachter**  
Lab Scientist  
Boehringer Ingelheim

**Teresa Puchner**  
Lab Scientist  
Boehringer Ingelheim

[Register Now](#)

Connect with us:

- [Search for Products](#)
- [Family of Brands](#)
- [Distributors](#)
- [Contact](#)



Bio-Techne  
614 McKinley Place NE, Minneapolis, MN USA 55413

If you no longer wish to receive messages from Bio-Techne you can unsubscribe at any time. You can update your communication preferences in our preference center.  
Copyright © 2023 Bio-Techne. All rights reserved.

## RESEARCH NOTE

# Parkinson's disease-linked V15A mutation facilitates $\alpha$ -synuclein aggregation by reducing membrane affinity

Fiamma A. Buratti<sup>1,2</sup> | Claudio Oscar Fernández<sup>2,3</sup> | Markus Zweckstetter<sup>1,3</sup>

<sup>1</sup>German Center for Neurodegenerative Diseases (DZNE), Göttingen, Germany

<sup>2</sup>Max Planck Laboratory for Structural Biology, Chemistry and Molecular Biophysics of Rosario (MPLbioR, UNR-MPINAT), Partner Laboratory of the Max Planck Institute for Multidisciplinary Sciences (MPINAT, MPG), Centro de Estudios Interdisciplinarios, Universidad Nacional de Rosario, Rosario, Argentina

<sup>3</sup>Department of NMR-Based Structural Biology, Max Planck Institute for Multidisciplinary Sciences, Göttingen, Germany

## Correspondence

Markus Zweckstetter, Department of NMR-Based Structural Biology, Max Planck Institute for Multidisciplinary Sciences, Am Fassberg 11, 37077 Göttingen, Germany.

Email: [markus.zweckstetter@dzne.de](mailto:markus.zweckstetter@dzne.de)

## Funding information

H2020 European Research Council, Grant/Award Number: 787679

**Review Editor:** Jean Baum.

## Abstract

Parkinson's disease can manifest either as a sporadic form, which is common, or as an inherited autosomal dominant trait resulting from missense mutations. Recently, the novel  $\alpha$ -synuclein variant V15A was identified in two Caucasian and two Japanese families with Parkinson's disease. Using a combination of NMR spectroscopy, membrane binding assays and aggregation assays we show that the V15A mutation does not strongly perturb the conformational ensemble of monomeric  $\alpha$ -synuclein in solution, but weakens its affinity for membranes. Attenuated membrane binding raises the concentration of the aggregation-prone disordered  $\alpha$ -synuclein in solution, allowing only the V15A variant but not wild-type  $\alpha$ -synuclein to form amyloid fibrils in the presence of liposomes. These findings, together with earlier research on other missense mutations of  $\alpha$ -synuclein, suggest that maintaining a balance between membrane-bound and free aggregation-competent  $\alpha$ -synuclein is critical in  $\alpha$ -synucleinopathies.

## KEYWORDS

aggregation,  $\alpha$ -synuclein, mutation, NMR, Parkinson's disease

## 1 | INTRODUCTION

Parkinson's disease (PD), the second most prevalent neurodegenerative disorder, is characterized by the loss of neurons in the substantia nigra and the accumulation of intracellular inclusions of  $\alpha$ -synuclein ( $\alpha$ Syn), the primary component of Lewy bodies (Poewe et al., 2017; Spillantini et al., 1997). While PD typically occurs sporadically, it can also be inherited as an autosomal dominant trait due to missense mutations. Although the

exact function of  $\alpha$ Syn remains unclear, it is widely acknowledged that it has a presynaptic location where it is linked with synaptic vesicles (Burré et al., 2010). Furthermore,  $\alpha$ Syn can promote the binding of SNARE complexes to phospholipids via its N-terminus (Maroteaux et al., 1988). When  $\alpha$ Syn binds to lipid membranes, its structure shifts from a random coil to an  $\alpha$ -helix (Davidson et al., 1998). In contrast,  $\alpha$ Syn is found as  $\beta$ -structure containing amyloid fibrils within Lewy bodies (Uéda et al., 1993).

This is an open access article under the terms of the [Creative Commons Attribution-NonCommercial-NoDerivs](https://creativecommons.org/licenses/by-nc-nd/4.0/) License, which permits use and distribution in any medium, provided the original work is properly cited, the use is non-commercial and no modifications or adaptations are made.

© 2023 The Authors. *Protein Science* published by Wiley Periodicals LLC on behalf of The Protein Society.

To date, nine potentially pathogenic variants of  $\alpha$ Syn associated with familial PD have been identified. This includes the well-studied A30P (Krüger et al., 1998), E46K (Zarranz et al., 2004) and A53T (Polymeropoulos et al., 1997) variants, as well as A30G (Liu et al., 2021), H50Q (Appel-Cresswell et al., 2013), G51D (Appel-Cresswell et al., 2013; Lesage et al., 2013), A53E (Pasanen et al., 2014), and A53V (Chen et al., 2020). In 2020, the novel  $\alpha$ Syn variant V15A was found in two Caucasian families with PD. (Minafra et al., 2020) Subsequently, the V15A mutation was identified in three affected individuals from two independent Japanese PD families with typical parkinsonism (Daida et al., 2022), suggesting a potential pathogenic role of the V15A  $\alpha$ Syn variant. Initial biochemical and aggregation experiments pointed to reduced affinity for phospholipids and increased fibril elongation activity for V15A  $\alpha$ Syn when compared with the wild-type (WT) protein (Daida et al., 2022). However, single-residue resolution information about the impact of the V15A mutation on the conformational ensemble of  $\alpha$ Syn, its membrane-binding and fibrillization in the presence of liposomes is unknown.

## 2 | RESULTS AND DISCUSSION

The structural features of the monomeric  $\alpha$ Syn WT and V15A protein were investigated by NMR spectroscopy and circular dichroism (CD). We examined the structural changes between the two proteins in aqueous solution by overlaying two-dimensional NMR  $^1\text{H}/^{15}\text{N}$ -correlation spectra. Both spectra displayed very similar amide group chemical shifts (Figure S1a) where most of the peaks overlapped except for the peaks corresponding to residues surrounding the mutation site (Figure S1b). This is consistent with the results from CD, where both spectra show a minimum at 198 nm, which is characteristic for random coil structure (Figure S1c). Residue-specific analysis of the secondary structure propensity of V15A  $\alpha$ Syn via  $\text{C}^\alpha$  secondary chemical shifts showed small perturbations close to the mutation site (Figure S1d). The data show that the V15A mutation does not strongly perturb the conformational ensemble of monomeric  $\alpha$ Syn in solution.

Next, we investigated the effect of the V15A mutation on  $\alpha$ Syn lipid interaction, by preparing liposomes from a mixture of DOPE:DOPS:DOPC (5:3:2 w/w). Dynamic light scattering showed that the size of the liposomes remained largely unaffected in the presence of  $\alpha$ Syn (Figure S2a). NMR spectroscopy was then used to examine the effect of the mutation on  $\alpha$ Syn's membrane binding ability in a residue-specific manner. We monitored the  $^1\text{H}/^{15}\text{N}$  signals in the presence of increasing liposome

concentrations (Figure S2b). Both proteins showed a similar binding profile (Figure S2c), with the 100 N-terminal residues experiencing an intensity decrease upon binding. However, this decrease in intensity was considerably less for the mutant. We also observed that the most liposome-perturbed protein region comprises the N-terminus from residues 1 to 25, which acts as a membrane anchor in  $\alpha$ Syn (Bodner et al., 2009; Fusco et al., 2014).

It is known that  $\alpha$ Syn adopts  $\alpha$ -helical conformation upon interaction with membranes. We therefore also used CD to compare the ability of both proteins to form  $\alpha$ -helical structure in the presence of increasing liposome amounts. The CD-based binding studies showed that the V15A  $\alpha$ Syn variant displays a lower propensity to fold into  $\alpha$ -helical structure in the presence of the liposomes (Figure S2d). Together with the observed decrease in NMR signal broadening, the data show that the V15A  $\alpha$ Syn variant has a lower membrane affinity when compared with the wild-type protein.

A decrease in membrane affinity by the V15A mutation is consistent with the location of V15 in the helical structure of  $\alpha$ Syn predicted by AlphaFold2 (Figure S2e, left). In the AlphaFold2-predicted  $\alpha$ -helix, the three hydrophobic residues F4, V15, and V26 are located on the same side of the helix with its side chains pointing into a similar direction. When  $\alpha$ Syn is bound to a membrane, these side chains are likely to insert into the hydrophobic environment of the lipid bilayer and thus anchor  $\alpha$ Syn to the membrane. Consistent with this hypothesis, the artificial F4A mutation attenuates  $\alpha$ Syn membrane binding (Lokappa et al., 2014), and evidence by continuous-wave EPR shows all the lipid-facing residues are generally hydrophobic (Jao et al., 2008). When V15 is replaced by alanine, one of the three hydrophobic membrane anchors is lost. In addition, less intramolecular interactions might be formed (Figure S2e, right), which could further contribute to the decreased membrane binding of the V15A  $\alpha$ Syn variant.

We next asked whether the decreased membrane affinity of V15A  $\alpha$ Syn, triggers  $\alpha$ Syn aggregation in the presence of a membrane, that is, in a situation possibly mimicking the pre-synaptic localization of  $\alpha$ Syn. To this end, we first characterized  $\alpha$ Syn fibrillization kinetics without liposomes (Figure 1a, left). In agreement with previous results (Daida et al., 2022), the kinetic parameters of fibrillization were very similar for WT and V15A  $\alpha$ Syn, with potentially a slight delay in aggregation of V15A  $\alpha$ Syn (Figure 1c). Electron microscopy and CD demonstrated the formation of  $\beta$ -structure containing amyloid fibrils (Figure 1b,d). However, when we incubated the proteins in the presence of liposomes (protein:lipid molar ratio 1:200), the situation drastically changed.

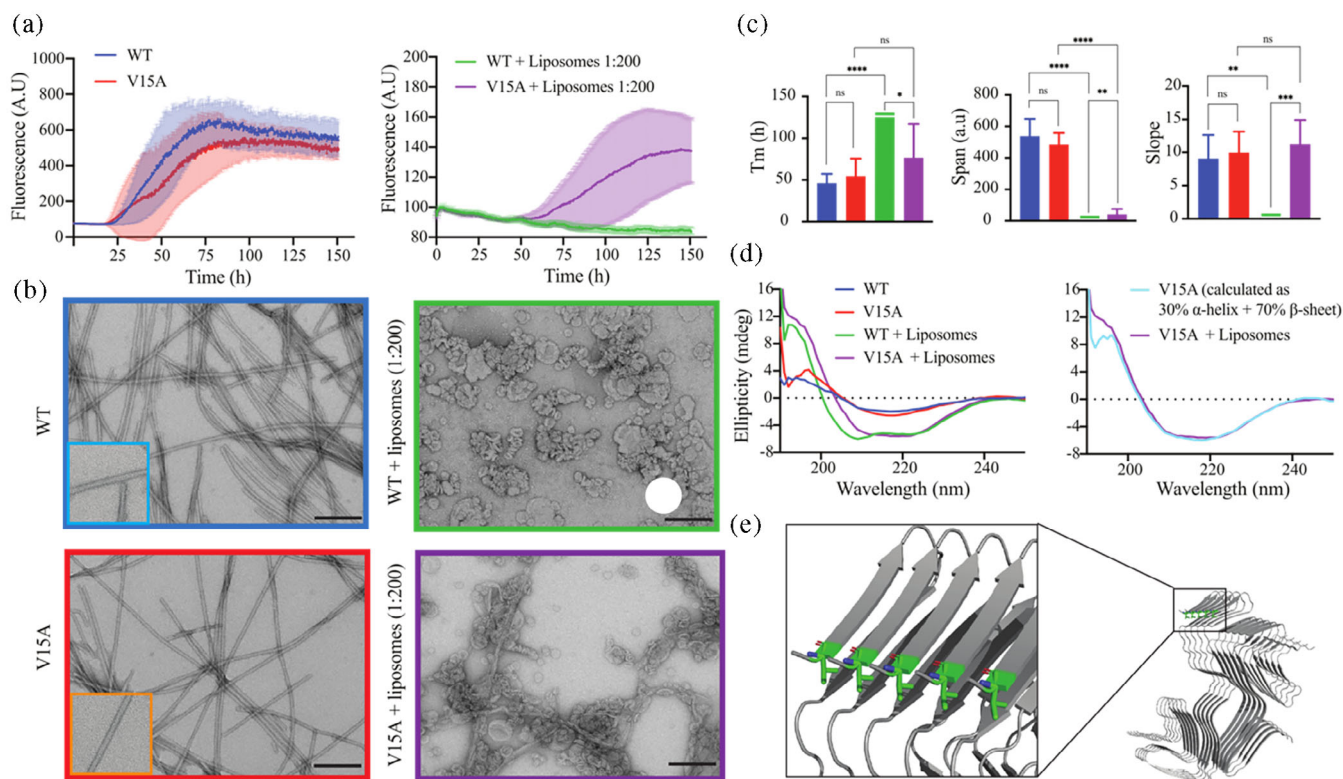


**FIGURE 1** V15A mutation facilitates  $\alpha$ Syn aggregation in the presence of liposomes. (a) Fibrillization kinetics of  $\alpha$ Syn WT (blue) and V15A (red) in solution (left), and in the presence of liposomes (right; WT/green and V15A/purple) measured by ThT fluorescence. Each curve represents the average of the group, error bars indicate std. (b) Electron micrographs of WT and V15A  $\alpha$ Syn after aggregation in the absence (left) or presence of liposomes (right). Scale bar, 200 nm. Insets show zoomed fibril views. (c) Parameters describing the kinetics of  $\alpha$ Syn aggregation in the absence (blue/WT, red/V15A) or presence of liposomes (green/WT, purple/V15A).  $T_m$  is the half-time of aggregation, span is the difference in fluorescence intensity at the start (bottom) and end of aggregation (top). Statistical analysis was conducted using  $t$  student test: ( $p < 0.05$ ) and non-significant (ns), significant (\*0.0109), (\*\*0.005), (\*\*\*)0.0009, (\*\*\*\*<0.0001). (d) CD spectra (left) of samples taken from the aggregation assay in (a) at the incubation end (left). (right) CD spectrum of V15A  $\alpha$ Syn in the presence of liposomes (purple) compared with a calculated curve (light blue) as a sum of 30%  $\alpha$ -helix and 70%  $\beta$ -sheet. (e) Cryo-EM structure of multiple system atrophy Type I  $\alpha$ Syn filament (PDB id: 6XYO) (Schweighauser et al., 2020). V15 is highlighted in green.

While the ThT signal of the V15A mutant started to rise after  $\sim 50$  h, WT  $\alpha$ Syn did not aggregate during the maximum time of incubation (150 h; Figure 1a, right). Electron microscopy confirmed the presence of fibril-like structures, together with liposomes, in the V15A  $\alpha$ Syn sample, but not for WT  $\alpha$ Syn (Figure 1b, right). The impaired ability of WT  $\alpha$ Syn to form fibrils in the presence of liposomes is likely because the concentration of free  $\alpha$ Syn monomer, that is, not bound to liposomes, is too low to trigger fibrillization during the incubation period. On the other, the decreased membrane affinity of the V15A variant of  $\alpha$ Syn results in an increase in free  $\alpha$ Syn monomer concentration exceeding the critical concentration for fibrillization.

The ThT intensity of V15A  $\alpha$ Syn aggregated in the presence of liposomes was significantly smaller than in the absence of liposomes (Figure 1a,c). This might be for a number of reasons including a lower fibril yield, a

different fibril structure or the partitioning of ThT into liposomes. Analysis of the CD spectrum of the V15A  $\alpha$ Syn sample, which was aggregated in the presence of liposomes, suggested  $\sim 70\%$   $\beta$ -structure and  $\sim 30\%$   $\alpha$ -helical content, indicating that a large fraction of V15A  $\alpha$ Syn was converted into amyloid fibrils. Regarding the structure of V15A  $\alpha$ Syn fibrils in the presence of liposomes, this is difficult to assess from the electron micrographs due to the close association of the fibrils with the liposomes (Figure 1b, right). Notably, the fibrils of V15A  $\alpha$ Syn formed in the absence of liposomes appeared less twisted than those of WT  $\alpha$ Syn (Figure 1b, left). This change in structure might arise from a loss of a stabilizing interaction of the side chain of V15, which is present at the N-terminal end of the resolved cryo-EM structure of multiple system atrophy Type I  $\alpha$ Syn fibrils (Schweighauser et al., 2020) (Figure 1e).

### 3 | DISCUSSION

The fact that all presently identified disease-linked mutations of  $\alpha$ Syn appear in its membrane binding domain supports a critical contribution of  $\alpha$ Syn/membrane interactions in  $\alpha$ -synucleinopathies. Nevertheless, the degree to which each disease-associated mutation impacts membrane binding can vary. For example, the A30P  $\alpha$ Syn variant shows decreased membrane binding because of reduced helix propensity (Fusco et al., 2016; Jo et al., 2002). In contrast, the E46K  $\alpha$ Syn variant may have stronger membrane affinity since the negative glutamate is replaced with a positive lysine resulting in enhanced electrostatic interactions with negatively charged membranes (Choi et al., 2004). In case of the V15A  $\alpha$ Syn variant, which has thus far been identified in four PD-affected families (Daida et al., 2022; Minafra et al., 2020), we observed decreased membrane binding affinity, despite the higher helix propensity of alanine as compared with valine. Structural modeling using AlphaFold2 suggested that the hydrophobic side chain of V15, together with the hydrophobic side chains of F4 and V26, is important for anchoring the  $\alpha$ -helix of  $\alpha$ Syn to membranes (Figure S2). The replacement of V15 with alanine therefore results in a decrease in membrane binding.

In neurons, a delicate balance likely exists between membrane-bound and freely diffusible  $\alpha$ Syn, with the distribution of protein between the two states being finely tuned (Runwal & Edwards, 2021). Our analysis reveals that the V15A mutation of  $\alpha$ Syn alters this balance by shifting the distribution from membrane-bound to free disordered protein (Figure S2). As demonstrated in our aggregation experiments (Figure 1), this shift can significantly impact  $\alpha$ Syn aggregation, given the strong dependence of aggregation on protein concentration. This proposed mechanism may also be relevant for the aggregation of wild-type (WT)  $\alpha$ Syn in sporadic PD. While the concentration of free  $\alpha$ Syn may be too low in young individuals to generate  $\alpha$ Syn inclusions, the gradual increase of free, aggregation-prone  $\alpha$ Syn concentration at older ages (e.g., due to neuronal aging) could lead to the development of pathogenic  $\alpha$ Syn inclusions.

### 4 | MATERIALS AND METHODS

#### 4.1 | Protein preparation

Protein expression and purification of human  $\alpha$ Syn was performed as previously described (Hoyer et al., 2002). V15A  $\alpha$ Syn was generated by site directed mutagenesis (QuikChange, Agilent). For the production of uniformly  $^{15}\text{N}$ -labeled samples, M9 minimal medium was used, supplemented with  $^{15}\text{NH}_4\text{Cl}$  (Sigma Aldrich). Finally,

proteins were dialyzed against the Nuclear Magnetic Resonance (NMR) buffer containing 100 mM NaCl, 50 mM HEPES, 0.02%  $\text{NaN}_3$ , pH 7.4.

#### 4.2 | Liposome preparation

2.5 mg of 1,2-Dioleoyl-sn-glycero-3-phosphoethanolamine (DOPE): 1.5 mg of 1,2-dioleoyl-sn-glycero-3-phospho-L-serine (DOPS): 1 mg of 1,2-dioleoyl-sn-glycero-3-phosphocholine (DOPC) 5:3:2 w/w (Avanti Polar Lipids) were prepared by drying a mixture of the different lipids dissolved in chloroform under a stream of  $\text{N}_2$  gas, lyophilized overnight and resuspended in 500 ml of HEPES buffer (50 mM HEPES, 100 mM NaCl, pH 7.4, 0.02%  $\text{NaN}_3$ ) to reach a final concentration of 15 mM. The resulting turbid sample was sonicated in a water bath until transparent (10 times 1 min with 3 min break). The size of the resulting liposomes (diameter of  $\sim 100$  nm) was determined by dynamic light scattering using a DynaPro NanoStar instrument (Wyatt Technologies Corporation).

#### 4.3 | NMR spectroscopy

NMR experiments were measured on a Bruker 700 MHz spectrometer equipped with a 5 mm triple-resonance, pulsed-field z-gradient cryoprobe using two-dimensional  $^1\text{H}$ ,  $^{15}\text{N}$  heteronuclear single quantum coherence (HSQC) (Bodenhausen & Ruben, 1980) for liposome titration, as well as  $^1\text{H}$ ,  $^{13}\text{C}$  heteronuclear single quantum coherence (HSQC) pulse sequences for monomer characterization at 15°C. All experiments were performed in HEPES buffer (50 mM HEPES, 100 mM NaCl, pH 7.4, 0.02%  $\text{NaN}_3$ ) with 10% (v/v)  $\text{D}_2\text{O}$ . The sample concentration for natural abundance  $^1\text{H}$ ,  $^{13}\text{C}$ -HSQC experiments was 100  $\mu\text{M}$  for both WT and V15A  $\alpha$ Syn. For the liposome titration experiments, the protein concentration was decreased to 40  $\mu\text{M}$  and individual samples prepared using a 15 mM liposome stock. Spectra were processed with TopSpin 3.6.1 (Bruker) and analyzed using Sparky 3.13 (T. D. Goddard and D. G. Kneller, SPARKY 3, University of California, San Francisco). The combined  $^1\text{H}/^{15}\text{N}$  chemical shift perturbation was calculated according to  $(\frac{((\delta_{\text{H}})^2 + (\delta_{\text{N}}/10)^2)}{2})^{1/2}$ .

#### 4.4 | Aggregation assay

The aggregation assay was performed on a TECAN Spark 20 M reader at 37°C with cycles consisting of 1 min shaking intervals followed by 10 min rest intervals over approximately 6.2 days (linear shaking amplitude: 6 mm, shaking frequency: 54 rpm). The Thioflavin T (ThT) fluorescence was

measured once every cycle for each well from the top (excitation wavelength: 440 nm, excitation bandwidth: 10 nm, emission wavelength: 482, emission bandwidth: 10 nm, gain level: 60, z-Position: 25658). Two beads per well.

Each condition (WT and V15A  $\alpha$ Syn) was measured with six replicates at 25  $\mu$ M of protein and 25  $\mu$ M of Thioflavin T concentration in HEPES buffer (50 mM HEPES, 100 mM NaCl, pH 7.4, 0.02%  $\text{NaN}_3$ ). The aggregation assay with liposomes was measured with four replicates at 25  $\mu$ M of protein, 5 mM of liposomes, and 25  $\mu$ M of Thioflavin T concentration in HEPES buffer (50 mM HEPES, 100 mM NaCl, pH 7.4, 0.02%  $\text{NaN}_3$ ).

#### 4.5 | CD spectroscopy

Individual WT and V15A  $\alpha$ Syn-to-liposome ratios were pipetted (ratio: 1:10, 1:20, 1:40, 1:100, and 1:200) at a protein concentration of 10  $\mu$ M and the respective liposome concentrations from a 15 mM liposome stock in water, total volume: 100  $\mu$ l. For CD measurement, 50  $\mu$ l of the sample was transferred to a 0.2 mm pathlength cuvette. CD data were collected from 190 to 250 nm by using a Chirascan-plus qCD spectrometer (Applied Photophysics, Randalls Rd, Leatherhead, UK) at 20°C, 1 time-per-point (s) in 1 nm steps. The datasets were averaged from three repeats. All spectra were baseline corrected against buffer in deionized water and smoothed (window size: 5).

#### 4.6 | Dynamic light scattering

Dynamic light scattering (DLS) measurements were performed at 25°C using a DynaPro NanoStar instrument (Wyatt Technologies Corporation). Liposome samples of 400  $\mu$ M in HEPES buffer (50 mM HEPES, 100 mM NaCl, pH 7.4, 0.02%  $\text{NaN}_3$ ) without and with 10  $\mu$ M WT and V15A  $\alpha$ Syn were measured in NanoStar disposable Micro-Cuvettes. They were illuminated with a 120 mW air launched laser of 662 nm wavelength and the intensity of 90° angle scattered light was detected by an actively quenched, solid-state Single Photon Counting Module (SPCM). Data were acquired with an acquisition time of 5 s and a total of 30 acquisitions per sample. Average values and their standard deviations were determined using the software package Dynamics 7.10.0.23.

#### 4.7 | Transmission electron microscopy (TEM)

Samples after aggregation were adsorbed onto 400 mesh carbon-coated copper grids and the buffer was removed

using a filter paper. Subsequently, samples were stained by the addition of 1% uranyl acetate solution, which was subsequently dried with a filter paper. The grids were imaged using a Talos L120C G2 electron microscope.

#### AUTHOR CONTRIBUTIONS

Fiamma A. Buratti performed NMR spectroscopy, biophysical experiments, and aggregation assays. Claudio Oscar Fernández and Markus Zweckstetter supervised Fiamma A. Buratti. Fiamma A. Buratti and Markus Zweckstetter wrote the manuscript. Markus Zweckstetter designed the project.

#### ACKNOWLEDGMENTS

We thank Prof. Dr. Katja Lohmann for making us aware of the novel  $\alpha$ -synuclein variant V15A, Maria-Sol Cima-Omori for recombinant protein production, and the electron microscopy facility of the Max Planck Institute for Multidisciplinary Sciences for electron micrographs. Fiamma A. Buratti thanks CONICET for fellowship and CUA-DAHZ. Markus Zweckstetter was supported by the European Research Council (ERC) under the EU Horizon 2020 research and innovation program (grant agreement No. 787679). Claudio Oscar Fernandez thanks Universidad Nacional de Rosario (UNR), FONCyT (PICT 201-74665), Ministerio de Educacion de Argentina and the Max Planck Society (P10390) for financial support. Open Access funding enabled and organized by Projekt DEAL.

#### CONFLICT OF INTEREST STATEMENT

The authors declare no conflict of interest.

#### DATA AVAILABILITY STATEMENT

All data that support the findings of this study are available from the corresponding authors upon request.

#### REFERENCES

- Appel-Cresswell S, Vilarino-Guell C, Encarnacion M, Sherman H, Yu I, Shah B, et al. Alpha-synuclein p.H50Q, a novel pathogenic mutation for Parkinson's disease:  $\alpha$ -synuclein p.H50q, a novel mutation for Pd. *Mov Disord*. 2013;28:811–3.
- Bodenhausen G, Ruben DJ. Natural abundance nitrogen-15 NMR by enhanced heteronuclear spectroscopy. *Chem Phys Lett*. 1980;69:185–9.
- Bodner CR, Dobson CM, Bax A. Multiple tight phospholipid-binding modes of  $\alpha$ -synuclein revealed by solution NMR spectroscopy. *J Mol Biol*. 2009;390:775–90.
- Burré J, Sharma M, Tsetsenis T, Buchman V, Etherton MR, Südhof TC.  $\alpha$ -Synuclein promotes SNARE-complex assembly in vivo and in vitro. *Science*. 2010;329:1663–7.
- Chen Y, Gu X, Ou R, Zhang L, Hou Y, Liu K, et al. Evaluating the role of *SNCA*, *LRK2*, and *GBA* in Chinese patients with early-onset Parkinson's disease. *Mov Disord*. 2020;35:2046–55.

- Choi W, Zibae S, Jakes R, Serpell LC, Davletov B, Anthony Crowther R, et al. Mutation E46K increases phospholipid binding and assembly into filaments of human  $\alpha$ -synuclein. *FEBS Lett.* 2004;576:363–8.
- Daida K, Shimonaka S, Shiba-Fukushima K, Ogata J, Yoshino H, Okuzumi A, et al.  $\alpha$ -Synuclein V15A variant in familial Parkinson's disease exhibits a weaker lipid-binding property. *Mov Disord.* 2022;37:2075–85.
- Davidson WS, Jonas A, Clayton DF, George JM. Stabilization of  $\alpha$ -synuclein secondary structure upon binding to synthetic membranes. *J Biol Chem.* 1998;273:9443–9.
- Fusco G, de Simone A, Gopinath T, Vostrikov V, Vendruscolo M, Dobson CM, et al. Direct observation of the three regions in  $\alpha$ -synuclein that determine its membrane-bound behaviour. *Nat Commun.* 2014;5:3827.
- Fusco G, Pape T, Stephens AD, Mahou P, Costa AR, Kaminski CF, et al. Structural basis of synaptic vesicle assembly promoted by  $\alpha$ -synuclein. *Nat Commun.* 2016;7:12563.
- Hoyer W, Antony T, Cherny D, Heim G, Jovin TM, Subramaniam V. Dependence of  $\alpha$ -synuclein aggregate morphology on solution conditions. *J Mol Biol.* 2002;322:383–93.
- Jao CC, Hegde BG, Chen J, Haworth IS, Langen R. Structure of membrane-bound  $\alpha$ -synuclein from site-directed spin labeling and computational refinement. *Proc Natl Acad Sci U S A.* 2008;105:19666–71.
- Jo E, Fuller N, Rand RP, St George-Hyslop P, Fraser PE. Defective membrane interactions of familial Parkinson's disease mutant A30P  $\alpha$ -synuclein 1. *J Mol Biol.* 2002;315:799–807.
- Krüger R, Kuhn W, Müller T, Woitalla D, Graeber M, Kösel S, et al. AlaSOPro mutation in the gene encoding  $\alpha$ -synuclein in Parkinson's disease. *Nat Genet.* 1998;18:106–8.
- Lesage S, Anheim M, Letournel F, Bousset L, Honoré A, Rozas N, et al. G51D  $\alpha$ -synuclein mutation causes a novel Parkinsonian-pyramidal syndrome: SNCA G51D in Parkinsonism. *Ann Neurol.* 2013;73:459–71.
- Liu H, Koros C, Strohäker T, Schulte C, Bozi M, Varvaresos S, et al. A novel SNCA A30G mutation causes familial Parkinson's disease. *Mov Disord.* 2021;36:1624–33.
- Lokappa SB, Suk J-E, Balasubramanian A, Samanta S, Situ AJ, Ulmer TS. Sequence and membrane determinants of the random coil-helix transition of  $\alpha$ -Synuclein. *J Mol Biol.* 2014;426:2130–44.
- Maroteaux L, Campanelli J, Scheller R. Synuclein: a neuron-specific protein localized to the nucleus and presynaptic nerve terminal. *J Neurosci.* 1988;8:2804–15.
- Minafra B, Buongarzone G, Gana S, Valente ML, Palmieri I, Biagini T, et al. A novel likely pathogenic SNCA variant associated with Parkinson's disease [abstract]. 2020. Available from: <https://www.mdabstracts.org/abstract/a-novel-likely-pathogenic-snca-variant-associated-with-parkinsons-disease/>
- Pasanen P, Myllykangas L, Siitonen M, Raunio A, Kaakkola S, Lyytinen J, et al. A novel  $\alpha$ -synuclein mutation A53E associated with atypical multiple system atrophy and Parkinson's disease-type pathology. *Neurobiol Aging.* 2014;35:2180.e1–5.
- Poewe W, Seppi K, Tanner CM, Halliday GM, Brundin P, Volkman J, et al. Parkinson disease. *Nat Rev Dis Primers.* 2017;3:17013.
- Polymeropoulos MH, Lavedan C, Leroy E, Ide SE, Dehejia A, Dutra A, et al. Mutation in the  $\alpha$ -synuclein gene identified in families with Parkinson's disease. *Science.* 1997;276:2045–7.
- Runwal G, Edwards RH. The membrane interactions of Synuclein: physiology and pathology. *Annu Rev Pathol Mech Dis.* 2021;16:465–85.
- Schweighauser M, Shi Y, Tarutani A, Kametani F, Murzin AG, Ghetti B, et al. Structures of  $\alpha$ -synuclein filaments from multiple system atrophy. *Nature.* 2020;585:464–9.
- Spillantini MG, Schmidt ML, Lee VM-Y, Trojanowski JQ, Jakes R, Goedert M.  $\alpha$ -Synuclein in Lewy bodies. *Nature.* 1997;388:839–40.
- Uéda K, Fukushima H, Masliah E, Xia Y, Iwai A, Yoshimoto M, et al. Molecular cloning of cDNA encoding an unrecognized component of amyloid in Alzheimer disease. *Proc Natl Acad Sci U S A.* 1993;90:11282–6.
- Zarranz JJ, Alegre J, Gómez-Esteban JC, Lezcano E, Ros R, Ampuero I, et al. The new mutation, E46K, of  $\alpha$ -synuclein causes Parkinson and Lewy body dementia: new  $\alpha$ -synuclein-gene mutation. *Ann Neurol.* 2004;55:164–73.

## SUPPORTING INFORMATION

Additional supporting information can be found online in the Supporting Information section at the end of this article.

**How to cite this article:** Buratti FA, Fernández CO, Zweckstetter M. Parkinson's disease-linked V15A mutation facilitates  $\alpha$ -synuclein aggregation by reducing membrane affinity. *Protein Science.* 2023;32(8):e4693. <https://doi.org/10.1002/pro.4693>